Resistive Tapered Stripline (RTS) in Electroencephalogram Recordings During MRI

Giorgio Bonmassar, *Member, IEEE*

***Abstract*—A purely resistive stripline lead is introduced to reduce the specific absorption rate (SAR) increase due to the presence of leads in electroencephalography (EEG) measurements during magnetic resonance imaging. Discontinuities in the resistivity profile of the stripline introduce high-frequency inductive impedance that is not present in the low-frequency band of the EEG recordings. The changes in SAR introduced by the resistive tapered stripline (RTS) are studied using the finite-difference time-domain (FDTD) algorithm on a spherical phantom that models the human head. The FDTD simulations predict a reduction of the peak SAR when using RTS versus conventional resistive carbon fibers. Furthermore, our FDTD simulations have been validated on a simple prototype that exhibits no temperature increase on a spherical phantom.**

***Index Terms*—Cable, electrocardiography, electroencephalography (EEG), finite difference time domain (FDTD), magnetic resonance imaging (MRI), specific absorption rate (SAR).**

I. Introduction

COMBINING electroencephalography (EEG) and magnetic resonance imaging (MRI) is becoming increasingly common both for basic neuroscience studies and clinical research [1]. In this paper, a technique based on equivalent lumped inductance (ELI) for building MRI-compatible EEG electrode leads has been developed.

The current tendency with advanced MRI such as **<Au. Pls. define fMRI.>** fMRI is to increase the signal-to-noise ratio (SNR) and resolution of the recordings by increasing the static field B_0. Higher RF (B_1) frequency systems are needed at higher B_0 because of the linear relation between Larmor frequency and B_0 field strength. This is a safety issue since the reduced penetration at higher frequencies requires higher RF power for imaging. Furthermore, EEG leads act as antennas, increasing the subject's RF power exposition [1]. From a safety perspective, the use of electrodes is in many respects similar to the presence of medical implants [2], [3] and wires [4]–[8] during MRI examinations. Most of the simulations showed that the increased heating of tissues due to the presence of a metallic implant depended on the dimensions, orientation, shape, and location of the implant in the patient. Increased heating of surrounding tissues is usually concentrated in a small volumetric area near the tip of the metallic wire. Specific absorption rate (SAR) peak values at individual points usually occur in nonuniform patterns depending on local gradients of conductivity, mass density, or proximity to RF sources. For example, using a head coil and normalizing the whole-body SAR to 1 W/kg, a value of 41 W/kg was obtained at this location when the absorption was averaged over 1 g of tissue, with a maximum value of 310 W/kg averaged over 1/8 g of tissue [5].

The published safety studies [9], [10] for EEG/fMRI involving SAR estimation and empirical measurements of tissue heating were performed at 1.5 T with metallic leads. These groups reported no significant temperature increase during a complete recording session on human subjects. However, recent studies [1] conducted at 3 and 7 T suggest that metallic leads may lead to elevated local and whole-head SAR values. Furthermore, there have been no systematic EEG/fMRI safety studies utilizing resistive cables or leads with resistors.

Standard electromagnetic interference (EMI) design rules [11] suggest using RF chokes or ferrite insulators on the leads to reject electromagnetic (EM) waves. Versions of such devices for electrophysiology have been successfully built and tested at 1.5 T [12].

In this design, we will introduce a similar inductive loading that requires a low amount of metal using purely resistive leads for potentially high $\vec{B}_0$ field applications. Furthermore, this technology can be used to produce EEG leads that are both of low impedance (e.g., compatible with conventional EEG leads) and MRI compatible.

II. Theory

The ELI is a key element in the design of high-speed circuits in which discontinuities in the signal and ground return path are used to reduce manufacturing costs [11]. In this study, ELI is used in the design of EEG leads to achieve high RF attenuation without introducing low frequency (LF) inductance and with negligible LF resistance. We introduce a lead with purely resistive loading called resistive tapered strip (RTS) to optimally convey to an amplifier [usually situated in an MRI suite (Fig. 1)] physiological signals in the microvolt range and with a frequency band of up to 50 kHz. Fig. 1 (*top*) shows the geometrical structure of RTS, which consists of resistive elements with sharp changes in conductivity (i.e., resistive discontinuities). In practice, RTS can be built by placing a thin layer ("$a \times b$") of

Manuscript received October 16, 2003; revised February 11, 2004. This work was supported by the United States Public Health Service National Institutes of Health under Grant 1R01EB002459-01.

The author is with the A. Martinos Center, Massachusetts General Hospital, Harvard Medical School, Charlestown, MA 02129 USA (e-mail: giorgio@nmr.mgh.harvard.edu).

Digital Object Identifier 10.1109/TMTT.2004.832688

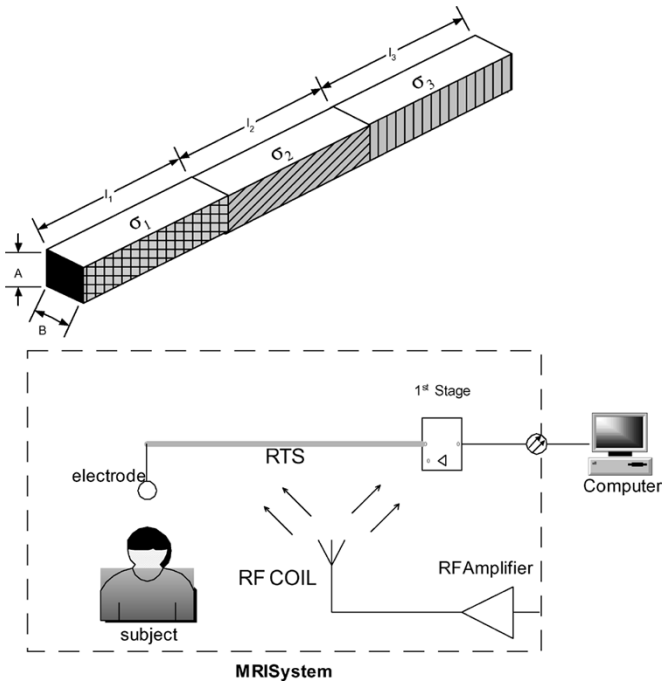

Fig. 1. (*top*) RTS can be made from solid copper and conductive polymer with different conductivity coefficients (e.g., σ_1, σ_2, and σ_3). (*bottom*) These fibers can be used to replace existing leads when measuring physiological signals during MRI.

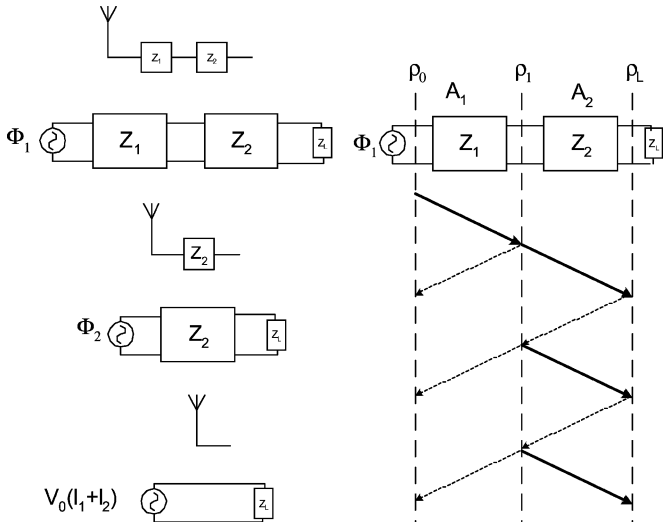

Fig. 2. Equivalent circuit used to study the RTS circuit. This hybrid circuit is composed of two parts: an antenna and a transmission line (left-hand side). This model considers the superposition of the effect of each layer of the RTS and the corresponding transmission line. The reflections that occur in the transmission line (right-hand side) characterize the overall impedance of the structure.

conductive ink for the length ("l_i") of each of the three resistive elements. The RTS can directly replace traditional leads (Fig. 1, *bottom*) in existing electrophysiological systems for MRI, and the high RF attenuation can reduce SAR and improve subject safety. (Fig. 1, *bottom*) depicts a human subject inside an MRI system with an attached EEG electrode set connected first a preamplifier through an EEG lead, then to a preamplifier, then to an optical decoupler, and finally to a system for EEG recording usually placed outside the MRI shielded room.

The RTS self-inductance is determined by the geometric relationship between the electrical circuit that transports the current I and the surface S_m through which the magnetic flux generated by I penetrates.

The proposed stripline can be represented with a hybrid model (Fig. 2) composed of an antenna attached to a transmission line. According to this model, the first antenna (i.e., the section of the RTS farthest from the subject) picks up the RF signal from the MRI and injects it into the first port of such a network (top left-hand side of Fig. 2). A portion of the power transmitted to the first layer of the RTS or port will be reflected back because of impedance mismatch between the first port and antenna, and a portion will be delivered to the second layer of the RTS or port. The second port is connected to a load that is intentionally mismatched to reflect part of the power back to the network and away from the human subject. In general, we need to consider the superposition of two opposite traveling steady-state sine waves: one forward directly generated by the excitation source and one backward from the mismatched boundary (Fig. 2, right-hand side).

The first step is to find the resistivity profile of the stripline. We will present a solution for a three-layer RTS based on the finite-difference time-domain (FDTD) algorithm (see below).

Each section "i" of the transmission line in Fig. 2 can be completely characterized by the following:

- impedance Z_{0i} (Ω);
- propagation constant γ_i;
- physical length l_i (M);
- Φ_1 is the maximum amplitude of the incident wave in the first discontinuity of the RTS (V).

This segment of RTS acts both as an antenna and transmission line for the signal that is reflected back from the subject. Using the same notation as in [13]

$$\Phi_1 = \sigma_1 l_1 \Delta H_{1x} - \rho_0\left(1 - \lambda_L^2 A_1^4 A_2^4 A_L^4\right) - \rho_1\left(A_1^2 - \lambda_L^2 A_1^2 A_2^4 A_L^4\right) - \rho_2\left(A_1^2 A_2^2 - \lambda_L^2 A_1^2 A_2^2 A_L^4\right) - \rho_L A_1^2 A_2^2 A_L^2 \quad (1)$$

where $\sigma_1 l_1 \Delta H_{1x}$ is the signal received by the first antenna of length l_1 since, for the short monopole approximation, the current is proportional to the monopole's length [14]. ρ_i is the reflection coefficient and $A_i = e^{-\lambda_i l_i}$ is the propagation term that incorporates the propagation constant λ_i and the length of each section l_i. Basically, (1) expresses the signal that is delivered to Z_L, which is the total signal received by the monopole $\sigma_1 l_1 \Delta H_{ox}$ minus the signal reflected back to the source Φ_1. The signal that emerges from the left-hand side of the port is the sum of all the terms that represent the intrinsic reflections in the RTS. The terms ΔH_{1x} (i.e., the variation of the magnetic field along the RTS or x-direction in the two adjacent Yee cells), ρ_i, and γ_i are estimated using the FDTD algorithm based on the particular geometrical model considered (in [13], actual measurements are performed instead). The total amount of the RF signal that reaches the subject is then found by superposition (Fig. 2, left-hand side) (using the same notation as in [13])

$$\Phi = \Phi_1 + \Phi_2 + \Delta H_{1x}(\sigma_1 l_1 + \sigma_2 l_2) \quad (2)$$

where

$$\Phi_2 = \sigma_2 l_2 \Delta H_{2x} - \rho_1\left(1 - \lambda_L^2 A_2^4 A_L^4\right) - \rho_2\left(A_2^2 - \lambda_L^2 A_2^2 A_L^4\right)$$

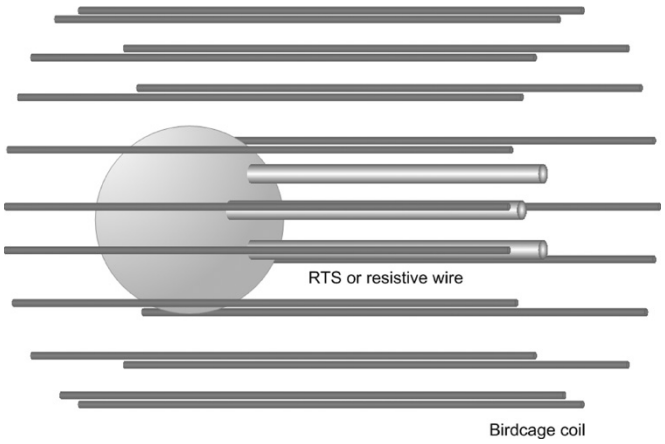

Fig. 3. 16-leg birdcage coil used in the RTS and carbon fiber simulations. The large sphere is the phantom representing the subject's head. The three large cylinders on top of the sphere represent either the RTS or the carbon fibers that are the EEG leads. The EEG electrodes are not represented in this model since we are considering the worst case of perfect contact between the subject's head and EEG lead.

$$-\rho_L A_2^2 A_L^2. \quad (3)$$

Equation (2) has four positive definite unknowns (conductivities and lengths of the RTS layers), which are: 1) σ_1; 2) σ_2; 3) l_1; and 4) l_2. Furthermore, there are additional minimization constraints on the upper limit (σ_T) of the positive RTS resistance and on the upper (L_2) and lower (L_1) limits of the total length

$$0 > \sigma_1 + \sigma_2 \geq \sigma_T \quad L_1 + \geq l_1 + l_2 \geq L_2. \quad (4)$$

The desired values of conductivities and lengths of the RTS can be found using constrained nonlinear optimization methods based on the Gauss–Newton and Lagrange multipliers. The complexity of the constrained minimization increases exponentially with the number of layers of the RTS.

III. Numerical Simulations

Here, we will first estimate the parameters of the equivalent circuit in Fig. 2 and then study the SAR behavior of the RTS fibers. The FDTD method is one of the most versatile approaches for EM modeling [15] and recent progress with the FDTD method has made it possible to perform very accurate calculations of S-parameters and coupling coefficients [14], [16].

The S_{11}-parameter and SAR simulations were estimated using the commercially available software XFDTD (REMCOM Company, State College, PA), based on the FDTD algorithm [14], [17] using the geometry shown in Fig. 3. A sphere (radius $r = 150$ mm) with a material with impedance approximately equal to gray matter of the brain (conductivity $\sigma = 0.6$ S/m, relative permittivity $\varepsilon_r = 80$, density $= 1030$ kg/m^3) was connected to an RTS made of three cylinders of sizes $l_1 = 80$ mm, $l_2 = 96.7$ mm, and $l_3 = 12$ mm and radii $r_{1,2,3} = 3$ mm, and with the conductances $\sigma_1 = 0.057$ S/m $\sigma_2 = \mathrm{PEC} \cdot \sigma_3 = 50$ S/m (see Fig. 1) all materials had $\varepsilon_r = 1$ and density $= 1000$ kg/m^3. In the SAR simulations, we used a total size of $210 \times 210 \times 450$ cells,

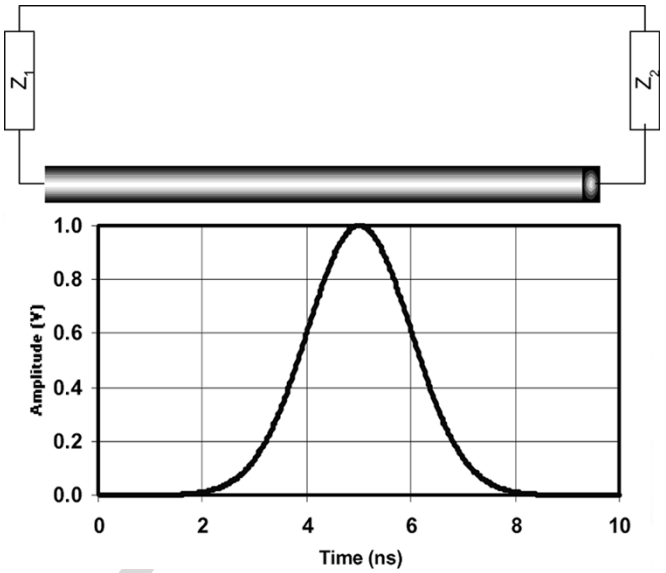

Fig. 4. (*top*) Schematics of the circuit and the (*bottom*) stimulus used to evaluate the S-parameters for the RTS.

a Yee cell resolution of $3 \times 3 \times 3$ mm^3, and "Liao"-type [14] absorbing boundary conditions.

A. S_{11}-Parameter

The FDTD algorithm has been successfully applied to constant a cross-sectional stripline to determine the equivalent circuit [18] and has been shown to provide a full-wave analysis tool for determining the EM field behavior. The RTS can be seen as a transmission line and both the propagation delay and impedances are dependent on the frequency of the RF field (Fig. 4, *top*).

The FDTD algorithm for the S-parameter estimation was set to perform 15 000 time steps or 16-ns duration. This number was obtained by testing convergence for port 1 versus time, and after 15 000 time steps, the transient response was back to zero. The stimulus source was a Gaussian pulse with a width of 1000 time steps or 1.6 ns. The pulsewidth is the number of Gaussian pulse half-amplitude time steps and the chosen values give a fairly flat representation in the LF to 300-MHz frequency band. (Fig. 4, *bottom*) shows the output of the Gaussian voltage source that was used as the active port in series with a 50-Ω resistor in the S-parameter simulations.

The resulting S_{11}-parameters' **<Au. Pls. define XFDTD.>** XFDTD computations confirmed that the RTS behaves predominantly as an inductor at our frequency of interest of 128 MHz (3 T).

B. SAR Simulation

SAR is the variable used in dosimetry to quantify the RF-tissue exposure. SAR is defined as the time derivative of the incremental energy absorbed by an incremental mass contained in a volume of a given density [19], [20], and is expressed in watts per kilogram. The relation between the SAR and electrical induced field is as follows [7], [21]:

$$\mathrm{SAR} = \frac{\sigma_e}{2\rho} \left| \vec{E} \right|^2 \quad (5)$$

where σ_e (in siemens per meter) is the electric conductivity, ρ ($\mathrm{kg/m^3}$) is the tissue density, and $\vec{E}$ (volts per meter) is the peak electric-field intensity inside the tissue.

The whole head averaged and peak values of SAR were computed in 140 000 steps. This number was found empirically verifying that stability of the electric field was reached. Stability is reached when the final time course is purely sinusoidal (i.e., no scattering) considering different cells on the sphere. The convergence of the SAR computations in XFDTD cannot be reached with a low number of steps, while a large number of steps does not lead to an error, but rather to unnecessary computing time. The active port (Fig. 4, *top*) was a sinusoidal current source with a frequency of 128 MHz (i.e., the Larmor frequency of our 3-T system) and amplitude of 1 V in parallel with a 50-Ω resistor. The averaging calculations were computed by XFDTD according to the methods described in [17]: cubical spaces centered on a cell are formed and the mass and average SAR of the sample cubes are found. The size of the sample cubes increases in odd-numbered steps to remain centered on the desired cell. The birdcage coil was composed of 16 perfect electric conductor (PEC) rods (length: 300 mm), closed by two PEC loops at each end (diameter: 270 mm, thickness: 3 mm) and placed symmetrically around the head [7], [21]. A circular excitation was simulated, driving the current generators placed on the centers of the rods with 1-A peak-to-peak amplitude and a 22.5° phase shift between any two adjacent generators.

We performed the following three simulations:

(#1) phantom with RTS;
(#2) phantom only;
(#3) phantom with conventional resistive leads (carbon fibers).

The model in simulation #3 was characterized with the same geometry as in simulation #1, but with only one cylinder ($l = 1000$ mm, $r = 10$ mm) with the following electrical parameters:

1) $\sigma = 0.2$ S/m;
2) $\varepsilon_r = 1$;
3) $\rho = 1000\ \mathrm{kg/m^3}$.

The total number of nonfree space cells for our model was 286 583 for simulations #1 and #3 and 286 357 for simulation #2. Yee cells contain six field components (E_x, E_y, E_z, H_x, H_y, and H_z, all offset by half a space step) used in the FDTD algorithm for a three-dimensional central-difference approximation of Maxwell's curl equations, both in space and time.

An Athlon MP2100 computer with 3.5 GB of RAM memory and dual processor was used for the calculations. The computation time was approximately 14 h for the 128-MHz SAR simulations and 45 min for the S-parameter estimation.

Fig. 5 shows some of the electric- and magnetic-field distributions estimated by FDTD in each of the three simulations. In particular, the $\left|\vec{\mathbf{B}}_{\mathbf{x}}\right|$ field distribution in the case of the carbon fiber (right-hand side, bottom) shows much larger RF currents everywhere. The $\left|\vec{\mathbf{E}}_{\mathbf{z}}\right|$ field distribution in the case of RTS (left-hand side, top) reveals a complex pattern that indicates the presence of reflections in and around the surfaces of resistive discontinuity.

Table I illustrates the behavior of RTS with respect to SAR and is compared to conventional carbon fibers. The FDTD simulations predict that there is a factor of two decrease in the peak SAR when using RTS relative to using normal carbon fibers normalized with respect to the total resistance of 3.2 Ω. This extremely low resistance of the carbon wires is uncommon in practice (introduced here only for illustration purposes); typically, carbon fibers exhibit resistance of a few kiloohms and will behave similarly to the RTS in reducing the peak SAR. Nevertheless, RTS can be successfully used to lower the LF resistance while maintaining high impedance at the RF frequency of interest.

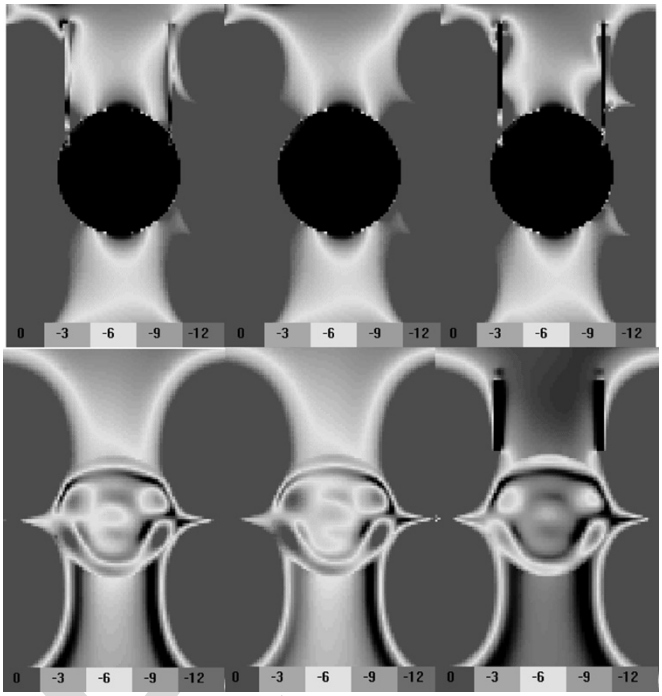

Fig. 5. (*top*) Magnitude of the electric field along the z-axis (0 dB $= 90$ V/m) and (*bottom*) magnitude of the magnetic field (0 dB $= 3.0\ 10^{-7}$ wb/m) along the x-axis. This figure was generated using: (first column) RTS, (second column) the bare phantom without any leads, and (third column) leads with uniform resistance.

IV. Experimental Results

A. Electrodes

We built EEG electrode sets using RTS fibers by making a simple two-layer prototype with a copper foil with conductive adhesive (P.N. 1181 EMI, 3M Corporation, Austin, TX) attached to a custom-made electrode set (VerMed Inc., Bellows Falls, VT). This electrode set was made of an 18-in lead conductive silver epoxy with a resistance of 50 Ω/in that covered a substrate of 0.2-in polyester transparent film, and the conductive epoxy was coated with an electrical insulating epoxy. At one end of the lead, a disposable cup electrode was attached to the polyester ring using silver epoxy and was surrounded by medical grade adhesive foam.

We also built EEG electrode sets using resistive wire (Fiberohm FO100P30P, 8.5 Ω/in$\pm$12%, Marktek Inc., Chesterfield, MO) that were matching the RTS prototypes both in length (i.e., 18 in) and total resistivity (i.e., 300 Ω) including the EEG paste (P.N. Z-181JE, Nihon Kohden Corporation, Tokyo, Japan). For both prototypes, the electrodes were the

TABLE I
RESULTS OF SAR NUMERICAL SIMULATIONS USING FDTD ESTIMATED @ 128 MHz OR 3-T FIELD. SIMULATIONS INCLUDED: 1) PURELY RESISTIVE LEADS (i.e., CARBON FIBERS); 2) NO LEADS; AND 3) RTS WITH SAME RESISTANCE OF THE RESISTIVE LEADS. THE SIMULATIONS SHOW THAT THE RTS HELP MAINTAIN THE PEAK SAR TO A VALUE VERY CLOSE (0.5%) TO THE NONLEAD CASE (i.e., PHANTOM ONLY) AND IS LOCATED NOT ON THE FIBER/SPHERE INTERFACE (27, 49, 91), BUT ON A POINT OF THE SPHERE

	RESISTIVE LEAD	PHANTOM ONLY	RTS
SAR peak (W/kg)	3.2	1.92	1.93
Peak-Position (x,y,z)	(27, 49, 91)	(48, 25, 84)	(48, 25, 84)
whole head SAR (W/kg)	0.07	0.07	0.07
Resistance (Ω)	3.3	-	3.3
Input Power (W)	1.09	1.07	1.16

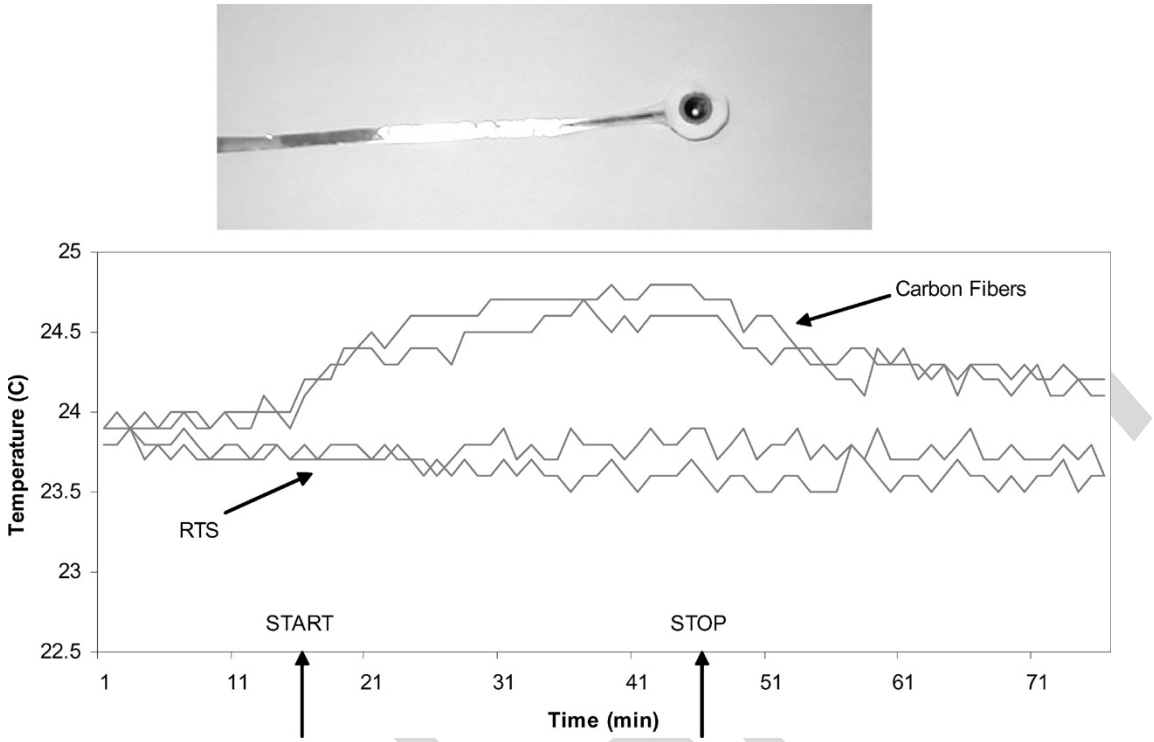

Fig. 6. (*top*) RTS prototype constructed using copper electrical tape (3M Corporation), conductive ink, and a conductive plastic electrode (VermMed Inc.). (*bottom*) Temperature graph measured using fluoroptic thermometer (Luxtron Corporation) placing two RTS and two carbon fibers on an agarose/conductive phantom. 15-min baseline was followed by 30 min of scanning and ending with 30 min of baseline. The two RTS fibers are clearly not producing any measurable heating, whereas the two carbon fibers are generating a temperature increase of approximately 0.5°.

same disposable cups (Model 36562, Plastics One, Roanoke, VA). The resistive wire FiberOhm was attached to the electrode using conductive epoxy (Circuit Works CW2400, Chemtronics, Kennesaw, GA).

B. Phantom

A phantom was prepared using a spherical glass bowl that was filled with 2 L of (boiling) solution of 25 g of agarose (Sigma Aldrich Inc., St. Louis, MO) and 2 g of NaCl. This phantom was built to allow placing of the electrodes on the conductive surface of the agarose through the opening of the bottle.

C. Measurements

We performed scanning on a Trio 3 Tesla MRI System (Siemens, Erlangen, Germany) running for 30 min a series of turbo spin echo (TSE) T1-weighted images with six slices, **<Au. "dist" correct as follows?>** dist factor of two, slice thickness of 30 mm, $\mathrm{TR} = 269$ ms, $\mathrm{TE} = 11$ ms, flip angle $= 130°$, field of view 250 mm × 100 mm, and a resolution of 512×256. These settings were chosen to achieve high RF power deposition and with a body weight of 150 lb the predicted whole-head average was 3.8 W/kg with a Siemens birdcage coil.

Temperature increases were recorded using a two-channel fluoroptic thermometer (Luxtron Corporation, Santa Clara, CA). The flurotopic-temperature probes were relayed inside the magnet through optical fibers and placed directly inside

the EEG paste of each disposable electrode cup. The electrodes/leads were then placed inside the glass bowl and firmly anchored between gel and glass. This entire setup rested for 1 h inside the bore of the magnet before the experimental session began.

D. Experiment

The temperature recording session started with 15 min of baseline measurement, followed by 30 min of scanning and ending with 30 min of baseline. There were two different temperature profiles observed (see Fig. 6) and the two RTS fibers clearly did not generate any measurable heating, whereas the two carbon fibers produced an increase of temperature of approximately 0.5°.

V. Summary

The concurrent measurement of fMRI and EEG will enable neuroscientists to study various physiological brain states, such as: 1) EEG waves; 2) sleep; 3) anesthesia and pharmacologically induced changes of brain activity; 4) in experiments for which there is no external task performance measure (e.g., covert word production, mental imagery, etc.); 5) in experiments that need to detect and quantify cognitive variables beyond paradigmatic control, such as state of attention or arousal; and 6) in experiments that investigate long-lasting learning or memory priming effects and that are irreproducible over multiple imaging sessions. Furthermore, it has potential applications in: 1) epilepsy research; 2) pediatric anesthesia; and 3) MRI guided surgery.

In this paper, we have described a new design for MRI use of EEG leads for low-impedance applications and low SAR that can potentially be applied more generally to electrophysiological recordings (e.g., EEG, electrocardiogram (EKG), etc.). Using simulations with a three-layer RTS, we have shown that it is possible to build a stripline that has the resistance of 3.2 Ω at LF and is capable of exhibiting an extremely low peak SAR at 128 MHz (3 T). RTS are directional and the peak SAR will depend on which end of the leads the subject will be connected. This structure can be built with purely conductive inks using a low overall resistivity, like the one used in EEG recordings. RTS is also useful in EEG/**<Au. Pls. define iEEG.>** iEEG recordings during RF exposures to study RF fields (mobile phone use) [22].

A simple prototype of RTS fibers was built and used in RF heating temperature measurements and no temperature increase using these fibers was recorded, even with high power deposition. However, a 0.5 °C temperature rise using traditional carbon fibers that were matched in geometry, length, and total impedance to the RTS fibers was recorded.

Within the limits of the simulations and the experimental results, it is suggested that RTS can be designed to achieve lower peak SAR levels than the traditional carbon lead fibers. However, further studies are needed to confirm that RTS are superior to traditional carbon fibers using: 1) realistic head models; 2) larger number of electrodes; 3) different field strengths; 4) coils; and 5) different layout/directionality of the fibers with respect to the B_1-field.

Acknowledgment

The author is grateful to J. Ackerman for many helpful discussions, P. Purdon for the custom-made resistive electrode set, and L. Angelone for making the phantom used in the T measurements, all with the A. Martinos Center, Massachusetts General Hospital, Harvard Medical School, Charlestown, MA. The author also thanks R. Luebbers, REMCOM Company, State College, PA, T. Vaughan of the **<Au. Pls. spell out CMRR.>** CMRR, University of Minnesota, **<City,>** for the prolific discussions, and G. Boas, A. Martinos Center, for his help in editing of this paper's manuscript.

References

[1] L. Angelone, A. Potthast, F. Segonne, S. Iwaki, J. Belliveau, and G. Bonmassar, "Metallic electrodes and leads in simultaneous EEG-MRI: Specific absorption rate (SAR) simulation studies," *Bioelectromagnetics*, vol. 25, pp. 285–295, 2004.

[2] J. D. de Certaines and G. Cathelineau, "Safety aspects and quality assessment in MRI and MRS: A challenge for health care systems in Europe," *J. Magn. Resonance Imaging*, vol. 13, pp. 632–638, 2001.

[3] F. G. Shellock, "Biomedical implants and devices: Assessment of magnetic field interactions with a 3.0-Tesla MR system," *J. Magn. Resonance Imaging*, vol. 16, pp. 721–732, 2002.

[4] M. F. Dempsey, B. Condon, and D. M. Hadley, "Investigation of the factors responsible for burns during MRI," *J. Magn. Resonance Imaging*, vol. 13, pp. 627–631, 2001.

[5] H. S. Ho, "Safety of metallic implants in magnetic resonance imaging," *J. Magn. Resonance Imaging*, vol. 14, pp. 472–477, 2001.

[6] J. Pictet, R. Meuli, S. Wicky, and J. J. van der Klink, "Radiofrequency heating effects around resonant lengths of wire in MRI," *Phys. Med. Biol.*, vol. 47, pp. 2973–2985, 2002.

[7] C. J. Yeung, R. C. Susil, and E. Atalar, "RF safety of wires in interventional MRI: Using a safety index," *Magn. Resonance Med.*, vol. 47, pp. 187–193, 2002.

[8] ——, "RF heating due to conductive wires during MRI depends on the phase distribution of the transmit field," *Magn. Resonance Med.*, vol. 48, pp. 1096–1098, 2002.

[9] L. Lemieux, P. J. Allen, F. Franconi, M. R. Symms, and D. R. Fish, "Recording of EEG during fMRI experiments: Patient safety," *Magn. Resonance Med.*, vol. 38, pp. 943–952, 1997.

[10] F. Lazeyras, I. Zimine, O. Blanke, S. H. Perrig, and M. Seeck, "Functional MRI with simultaneous EEG recording: Feasibility and application to motor and visual activation," *J. Magn. Resonance Imaging*, vol. 13, pp. 943–948, 2001.

[11] H. Johnson and M. Graham, *High-Speed Digital Design, A Handbook of Black Magic*. Upper Saddle River, NJ: Prentice-Hall, 1993.

[12] M. E. Ladd and H. H. Quick, "Reduction of resonant RF heating in intravascular catheters using coaxial chokes," *Magn. Resonance Med.*, vol. 43, pp. 615–619, 2000.

[13] C. Abernethy, A. Cangellaris, and J. Prince, "A novel method of measuring microelectronic interconnect transmission line parameters and discontinuity equivalent electrical parameters using multiple reflections," *IEEE Trans. Comp., Packag., Manufact. Technol. B*, vol. 19, pp. 32–40, Feb. 1996.

[14] A. Taflove and S. C. Hagness, *Computational Electrodynamics: The Finite-Difference Time-Domain Method*, 2nd ed. Boston, MA: Artech House, 2000.

[15] R. Mittra, S. Chebolu, and W. Becker, "Efficient modeling of power planes in computer packages using the finite difference time domain method," *IEEE Trans. Microwave Theory Tech.*, vol. 42, pp. 1791–1795, Sept. 1994.

[16] T. Itoh and B. Houshmand, *Time-Domain Methods for Microwave Structures: Analysis and Design*. Piscataway, NJ: IEEE Press, 1998.

[17] K. S. Kunz and R. J. Luebbers, *The Finite Difference Time Domain Method for Electromagnetics*. Boca Raton, FL: CRC, 1993.

[18] W. Becker, P. H. Harms, and R. Mittra, "Time-domain electromagnetic analysis of interconnects in a computer chip package," *IEEE Trans. Microwave Theory Tech.*, vol. 40, pp. 2155–2164, Dec. 1992.

[19] C. K. Chou, H. Bassen, J. Osepchuk, Q. Balzano, R. Petersen, M. Meltz, R. Cleveland, J. C. Lin, and L. Heynick, "Radio frequency electromagnetic exposure: Tutorial review on experimental dosimetry," *Bioelectromagnetics*, vol. 17, pp. 195–208, 1996.

[20] "Biological effects and exposure criteria for radiofrequency electromagnetic fields," NCRP, Bethesda, MD, vol. 86, 1986.
[21] J.-M. Jin, *Electromagnetic Analysis and Design in Magnetic Resonance Imaging*. Boca Raton, FL: CRC, 1999.
[22] R. Huber, J. Schuderer, T. Graf, K. Jutz, A. Borbely, N. Kuster, and P. Achermann, "Radio frequency electromagnetic field exposure in humans: Estimation of SAR distribution in the brain, effects on sleep and heart rate," *Bioelectromagnetics*, vol. 24, pp. 262–276, 2003.

Giorgio Bonmassar (S'89–M'90) was born in Milan, Italy, on May 13, 1962. He received the Dr.Eng. degree in electronics from the University of Rome "La Sapienza," Rome, Italy, in 1989, and the Ph.D. degree in biomedical engineering from Boston University, Boston, MA, in 1997.

From 1989 to 1991, he was a Research and Development Systems Engineer with Ericsson, Rome, Italy, a Research Fellow (1992–1997) and a Post-Doctoral Fellow (1997) with Boston University, Boston, MA, and a Research Fellow (1998–2000) with Massachusetts General Hospital, Boston, MA. Since 2000, he has been an Instructor with the Harvard Medical School (MGH), Boston, MA. He has authored or coauthored over 60 international journal papers and conference presentations on biomedical engineering.

Dr. Bonmassar is a member of the International Society for Magnetic Resonance Imaging and the Alfa Eta Mu Beta Biomedical Engineering Research Society. He was the recipient of a 1999 North American Treaty Organization (NATO) Advanced Research Studies Award and a 2000 Whitaker Foundation Biomedical Engineering Grant for Young Investigators. Since 2003, he is the **<Au. Pls. define PI.>** PI on a **<Au. Pls. define NIBIB.>** NIBIB–National Institutes of Health (NIH) grant.